Robust Decentralized Dynamic State Estimation Considering Instrumentation Chain Anomalies

Abdul Saleem Mir, Abhinav Kumar Singh, *Member IEEE* and Nilanjan Senroy, *Senior Member IEEE*

***Abstract*— A decentralized method for estimating the interior states of a synchronous machine using analogue measurements from instrument transformers (that is, current transformer and potential transformer) has been proposed in this paper. The method is robust to instrumentation chain anomalies, which have not been considered in the existing dynamic state estimation literature. The method works in a two-step manner, wherein a robust adaptive detection scheme removes instrument transformer anomalies, harmonics, noise, and DC components, and estimates the phasors of the analogue measurements, and subsequently uses these estimated phasors in the decentralized dynamic state estimation algorithm. Robust and adaptive version of square-root-cubature-Kalman-filter has been employed to enhance estimation accuracy irrespective of the type of noise distribution. The superiority of the algorithm over existing methods has been established in terms of numerical accuracy, computational efficacy, and robustness. IEEE 68 bus power system has been used to test the effectiveness of the developed strategy. Opal-RT based setup has also been used to implement the case studies in real-time.**

***Index Terms*— Automatic voltage regulator (AVR), Control, Dynamics, Estimation, Instrument Transformer, Lyapunov, Power System Stabilizer (PSS), Phasors, Synchronous machine.**

NOMENCLATURE

$k = k^{th}$ *instant of time,* $p = p^{th}$ *machine.*

ω_B, ω	Base elec. speed (*rad/s*), machine speed in *p.u.*
f_{V}, f_1	Stator voltage (V) freq. in *p.u*, fundamental freq.
$\mathrm{P_e}$, $\mathrm{I_e}$	Electrical power and stator current resp.
δ, θ	Rotor angle and stator voltage phase angle in *rad.*
V_a, E_{fd}	AVR regulator voltage, field excitation voltage
V_r, V_s	AVR filter voltage and PSS output resp.
e'_d, e'_q	Transient *d* and *q* axis emfs in *p.u.*
ψ_d, ψ_q	Subtransient damper coil *d* and *q* axis emfs in *p.u.*
$p_{i=1\ldots3}$	PSS states, f_{I} =frequency of the stator current.
v_q, v_d	*q* and *d* axis stator voltages ($\mathrm{V}_t = v_d + jv_q$) in *p.u.*
i_q, i_d	*q* and *d* axis stator currents ($\mathrm{I}_e = i_d + ji_q$) in *p.u.*
$\boldsymbol{x}$, $\boldsymbol{u}$	State and pseudo-input vectors respectively
$\boldsymbol{y}$, n_x	Measurement vector, State vector dimension.
$s(t)$	Instantaneous CT/PT measurement
$\boldsymbol{s}$, $\boldsymbol{q}$	Process and pseudo-input noise vectors resp.
$\boldsymbol{r}$	Column vector of noise in measurement vector
$\mathcal{P}_x$, $\mathcal{P}_y$	State and measurement covariance matrices resp.
$\mathcal{P}_{xy}$	Cross-correlation covariance matrix
$\mathcal{P}_{xq}$	Cross-covariance matrix of $\boldsymbol{x}$ and $\boldsymbol{q}$
$\mathcal{P}_\xi$	$= [\mathcal{P}_x\ \mathcal{P}_{xq}^{\mathrm{T}}\ ;\ \mathcal{P}_{xq}\ \mathcal{P}_q]$, n_m = no. of syn. machines.
Q_ξ	Constant additive process noise covariance matrix
R_y	Constant measurement noise covariance matrix
$\mathrm{T_s}$, n_y	Sampling time (s), Number of measurements
Tria (.)	General triangularization algorithm

I. INTRODUCTION

DUE to the variability in stochastic generation, random disturbances and fewer enhancements in the network at the bulk transmission level, synchronous generators of the interconnected power systems are under continuous stress. Stressed power systems are prone to outages and a disturbance can initiate undesirable oscillations [1]. Control and monitoring of instabilities and related dynamics require real-time estimation of the synchronous machine operating state. In this context, dynamic state estimation (DSE) is an effective tool in assessing dynamic security, monitoring oscillations and in enhancing system control [2]-[3].

The reliability of DSE based on synchrophasors data relies heavily on the accuracy of the phasors computed by PMUs [3]-[8]. Time synchronization in PMUs (which is used to generate a rotational reference frame for power systems) introduces time synchronization-errors, which not only increases the total vector error (TVE) of PMU measurements, but also introduces gross bad-data [6]-[8]. Due to the non-Gaussian nature of the PMU measurement noise [9] dynamic estimates via Bayesian filters [10]-[11] may not be accurate as they fundamentally assume Gaussian noise statistics. Additionally, PMUs are vulnerable to cybersecurity threats, like time synchronizing spoofing, packet sniffing, and malicious code data injection attacks [7]. These errors can propagate through the estimation process and may lead to erroneous estimates, thereby compromising the accuracy of DSE. DSE's dependence on time synchronization can be removed by replacing the synchronous machine rotor angle in the dynamic model by a relative angle [5], [12]. Using this paradigm, all the states of the synchronous machine can be estimated without any need of time synchronization of measurements. Apart from aforementioned errors, problems in DSE emanate due to inaccuracy in PMU phasor measurements, which in turn is linked to accuracy of measurement instrumentation system (a prime source of gross errors) [13]-[14]. Therefore, robust and accurate phasor parameter estimation using local measurements from instrument transformers is required by addressing signal modelling inaccuracies. These phasor parameter estimates can then be utilized in a second stage to find the machine states using decentralized dynamic state estimation (DDSE).

Interpolated discrete Fourier transform (IDFT) based DSE has been proposed for estimation of states using such a two-step procedure [5]. But, like PMU based DSEs [4], [15]-[16],

This is the author's accepted manuscript (AAM) version of DOI 10.1109/TPWRS.2022.3230842.
This work was supported by EPSRC UK under Grant EP/T021713/1.
Abdul Saleem Mir is with the Department of Electrical Engineering, Indian Institute of Technology Roorkee, India; (email; saleemmir@ee.iitr.ac.in), Abhinav Kumar Singh is with the School of Electronics and Computer Science, University of Southampton, UK (email: a.k.singh@soton.ac.uk), and Nilanjan Senroy are with the Department of Electrical Engineering, Indian Institute of Technology Delhi, India; (email: nsenroy@ee.iitd.ac.in).

IDFT based DSE [5] may not produce accurate estimates as actual field measurements are contaminated with non-Gaussian noise, structural/non-structural outliers, distortions and decaying DC-anomalies (DDA) which are not addressed explicitly in IDFT design. Therefore, robustness to structural/non-structural outliers, non-Gaussianity and DDAs needs to be addressed both in the phasor estimation stage as well as in the DDSE stage for accurate estimation of machine states.

For the phasor estimation stage, many DFT based options are available in the literature besides [5], such as windowed interpolation DFT [17]. Their performance worsens due to measurement fluctuations and the problems like picket fence effects and spectral leakage may impair their accuracy [14]-[16]. Other state-of-the-art methods like notch filters, and observer methods do not perform well for the duration of transient conditions, and it could hamper its real-time applicability [17]-[19]. Likewise, Taylor-Kalman methods and associated algorithms [20] suffer from signal modelling inaccuracies and are not robust to amplitude/phase jumps, which are a consequence of tap change, generation/load/line switching, and stepped variations in power through reactive components (overhead line and transformers). New enhancements [21]-[22] have been reported to be effective wherein harmonics and DDA effects have partially been explored/addressed. However, in these methodologies the model time constant selection for DDA is arbitrary and measurement chain transfer function inverse (MCTFI) [13] is required to alleviate the effect of unaccounted anomalies and measurement distortions. Numerous techniques [23]-[25] have been reported in the literature to mitigate and filter out the instrumentation chain errors in the measured signal. In [23], wavelet transform has been employed to compensate the effect of saturation. A method based on least square filter has been applied to mitigate transient errors [24]. The performance of these techniques relies heavily on the prior information of the instrumentation chain model and filter characteristics. Artificial neural network (ANN) based error correction method has been proposed in [25]. However, using ANN based correction method may not be feasible for real-time applications. To address these issues, adaptive detection scheme (ADS) has been proposed in this paper as a precursor for DSE, which efficiently mitigates the impact of the distortions like DDAs, harmonics and noise.

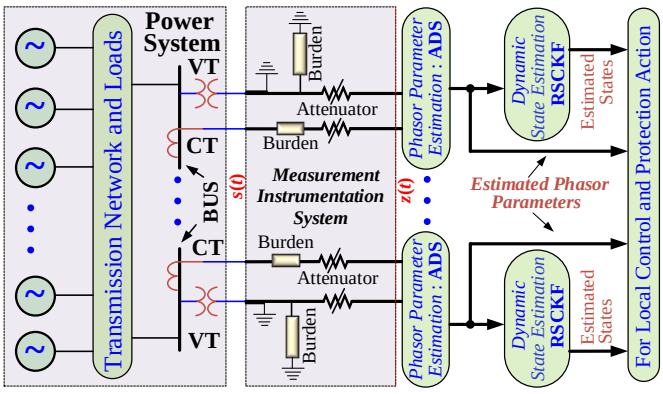

Fig. 1: Schematic of the methodology.

For the DSE stage, generic Bayesian filters like UKF suffer from curse-of-dimensionality and divergence [11]. Also, the computational cost, truncation error and numerical stability of the UKF family depend upon the number/weight of sigma points in the sigma set [11]. Square-root CKF (SRCKF) [10], [26] and its variants [10], [26]-[27] address these issues mentioned in [11]. However, these methods also fail to deal with observation, innovation, and structural outliers, and assume Gaussian statistics of noise and bad data in the measurement vector. Other non-Gaussian filters are computationally expensive and suffer from particle degeneracy and impoverishment problems [28]. Particle filters are sensitive to parametric variations and initial conditions, and are also susceptible to divergence [15], [16]. These discrepancies were partially addressed in algorithms like GMUKF [15], GMIEKF [16] wherein Huber projection statistics have been used [27]. Similar enhancements have been suggested in [27], [30]. However, performance indices of these filters may deteriorate if measurement noise characteristic changes from non-Gaussian to Gaussian.

The performance of DDSE can be effectively enhanced by reformulating the measurement information via its regression model and using Gaussian kernel with adaptive width. The notion behind using this formulation (unlike [27]-[31]) is to enhance the stabilization/accuracy of the trajectory of the estimates irrespective of the noise statistics. Accordingly, and also to address other aforementioned issues in measurement chain, a two-step procedure has been proposed in this paper (Fig. 1): (*a*) ***Precursor***: robust adaptive detection scheme (ADS) for estimation of amplitude, frequency, and phase of currents/voltages for use in the measurement model of DDSE and (*b*) ***Successor***: an enhanced adaptive robust square-root CKF (RSCKF), for the estimation of the states of the synchronous machine. The robust nonlinear observer-based ADS proposed in this paper ensures extenuation of tailed impulsive noise, DDAs and measurement outliers, and effective harmonic neutralization. It also removes the requirement of prior knowledge of MCTFI [13].

The proposed methodology has been evaluated on the 16 machine 68 bus power system [4]. The key advantages/ contributions of this paper are enumerated below.

- A Lyapunov criterion based robust ADS has been derived and used to estimate the generator bus current/voltage phasor parameters. ADS, unlike currently available methods ([5] and [17]-[22]), by design is robust to measurement distortions like amplitude/phase jumps, harmonics, DDA and non-Gaussian noise. Additionally, it eliminates the requirement of MCTFI [13] (otherwise required) to tackle unaccounted anomalies.
- The convergence of ADS method is assured under disturbances, unlike presently available state-of-the-art methods [5], [17]-[22]. The convergence of the phasor parameters is corroborated by the standard *persistence-of-excitation* condition [19].
- Subsequent DDSE stage uses a modified version of SRCKF [26], robustness of which was enhanced by making the measurement covariance matrix a numerically stable and adaptive exponential function of innovation square. Compared to enhancements in the literature [26]-[30], the adaptively enhanced RSCKF is numerically stable and demonstrably better, particularly

when the measurement noise is impulsive and/or measurement error is too high or too low. It uses a regression model and an adaptive Gaussian kernel for measurement covariance matrix modulation to enhance accuracy regardless of the nature of noise statistics.

- The proposed method, being decentralized, is not affected by system size and its stability is proven without any assumption about the linearity of the measurement model, as in [32]. The relationship between the state vector dimension and observability [33] is also explored.
- The bias and standard errors of the proposed DDSE are consistently and significantly lower than presently available methods in the literature [5], [17]-[22].
- Proposed ADS-DDSE uses generator bus measurements and is therefore particularly effective for realization of decentralized control methodologies as it doesn't require any synchrophasor measurement device (that is, PMUs) for its implementation [12], [30], [34]-[35].
- Practical applicability has been demonstrated using a scaled lab setup using Opal-RT multiprocessors.

The rest of the paper is organized as follows: after discussing the problem formulation in Section II and measurement signal model in Section III, the ADS methodology and DDSE algorithm are discussed in Section III and Section IV respectively. Filter stability, and the case studies are presented in Section V, and Section VI respectively whereas the conclusions are presented in Section VII.

II. Problem Description and Formulation

DDSE is implemented at each machine of the connected power system and it uses analogue measurements from the terminal bus measurement transformers. In this paper, a detailed sub-transient model of 16 machine 68 bus system (Fig. A1 in the Appendix, [4]) has been considered. The first eight machines of the test system have IEEE-DC1A type of automatic voltage regulator (AVR). The 9th machine has IEEE-ST1A AVR and a power system stabilizer (PSS) whereas rest of the machines have manual exciters. The model decoupling approach for DDSE has been adapted from [12]. For the p^{th} machine ($1 \le p \le n_m$) the decoupled process and measurement equations for use in the DDSE assume the composite state-space form as follows.

$$\dot{\boldsymbol{x}} = \boldsymbol{f}(\boldsymbol{x},\boldsymbol{u}) + \boldsymbol{s}, \quad \boldsymbol{y} = \boldsymbol{g}(\boldsymbol{x},\boldsymbol{u}) + \boldsymbol{r} \tag{1}$$

where, $\boldsymbol{f}$ and $\boldsymbol{g}$ are the process and measurement functions respectively. In decentralized augmented form, the process and the measurement equations (not detailed here due to space constraints) of the p^{th} machine are written in discrete form as follows [4], [5].

$$\boldsymbol{\xi}_k = \boldsymbol{f}_p(\boldsymbol{\xi}_{k-1},\boldsymbol{u}_{k-1}) + \boldsymbol{s}_{k-1} \tag{2}$$

$$\boldsymbol{y}_k = \boldsymbol{h}_p(\boldsymbol{\xi}_k,\boldsymbol{u}_k) + \boldsymbol{r}_k\,;\ \boldsymbol{\xi}_k = [\boldsymbol{x}_k \quad \boldsymbol{q}_k]^{\mathrm{T}}$$

$$\boldsymbol{x}_k = \left[\alpha_k\ \omega_k\ e'_{dk}\ e'_{qk}\ \psi_{dk}\ \psi_{qk}\ \mathrm{V}_{rk}\ \mathrm{V}_{ak}\ \mathrm{E}_{fdk}\right]^{\mathrm{T}};\ p = 1,\ldots,8$$

$$\boldsymbol{x}_k = \left[\alpha_k\ \omega_k\ e'_{dk}\ e'_{qk}\ \psi_{dk}\ \psi_{qk}\ \mathrm{E}_{fdk}\ p_{s1k}\ p_{s2k}\ p_{s3k}\right]^{\mathrm{T}};\ p = 9$$

$$\boldsymbol{x}_k = \left[\alpha_k\ \omega_k\ e'_{dk}\ e'_{qk}\ \psi_{dk}\ \psi_{qk}\ \right]^{\mathrm{T}};\ p = 10,\ldots,16$$

where, $\alpha_k = \delta_k - \theta_k$, $\boldsymbol{y}_k = \left[\mathrm{P}_{e,k}\ \mathrm{I}_{ek}\right]^{\mathrm{T}}$, $\mathrm{P}_{e,k} = \mathrm{V}_{d,k}\mathrm{I}_{d,k} + \mathrm{V}_{q,k}\mathrm{I}_{q,k}$, $\mathrm{I}_{ek} = (\mathrm{I}_{d,k}^2 + \mathrm{I}_{q,k}^2)^{1/2}$, column vector of noise in y_k is $\boldsymbol{r}_k = \left[\tilde{\mathrm{P}}_{e,k}\ \tilde{\mathrm{I}}_{e,k}\right]^{\mathrm{T}}$, pseudo input $\boldsymbol{u}_k = \left[\mathrm{V}_k\ f_{\mathrm{V},k}\right]^{\mathrm{T}}$, column vector of noise in $\boldsymbol{u}_k$ is $\boldsymbol{q}_k = \left[\tilde{\mathrm{V}}_k\ \tilde{f}_{\mathrm{V},k}\right]^{T}$ and $\boldsymbol{s}_{k-1}$ is the process noise vector. The measurements $\boldsymbol{y}_k$ and the pseudo-inputs $\boldsymbol{u}_k$ are derived from ADS based parameter estimator.

A. *Instrument Transformer Models for Analogue Measurement Generation*:

The IEEE Power System Relaying Committee (PSRC) recommendations and relevant task force guidelines [36] were followed to simulate the effect of instrumentation chain on the transmitted measurements. The IEEE PSRC committee has proposed instrumentation transformer models based on the assumption of the single-valued saturation curve. Details of the PT/CT models are given in [36], [37]. Nonlinear characteristics of the magnetic core in the CT model is based on the Jiles-Atherton principle [37] of ferromagnetic hysteresis. IEEE PSRC CT model is briefly discussed in Appendix-A.

Signal parameters (amplitude, frequency and phase of the current transformer (CT) currents and potential transformer (PT) voltages) estimated from analogue measurements using ADS algorithm (Section-III) are used to derive the necessary inputs $\boldsymbol{u}_k = \left[\mathrm{V}_k\ f_{\mathrm{V},k}\right]$ and measurements $\boldsymbol{y}_k = \left[\mathrm{P}_{e,k}\ \mathrm{I}_{ek}\right]$ for use in the subsequent DDSE algorithm (Section-IV). It should be noted here that the ADS algorithm for signal parameter estimation is model agnostic and therefore does not require modelling details of the instrumentation chain.

III. Instrumentation Chain And Signal Model

Errors in the measurements stem from the measurement chain (which includes instrumentation/control cables, instrument transformers (ITs), and associated burdens; Fig. 1. In some cases, IT saturates due to the characteristics of its core, and it generates harmonics on its own. IT core saturation, length of instrumentation/control cables and possibly high burden contribute to the errors [13]-[14]. Inaccurate phasor measurements stem due to the application of poorly fit model of the signal, as they do not consider the aforementioned distortions.

The signal model should be general to account for the aforementioned distortions, and appropriately capture the IT core nonlinearities. Alternating current saturation can be captured by choosing sufficiently large harmonic order, n, whereas direct current saturation effect can be represented by a decaying DC component in the signal model. Common causes of the DC saturation are faults, IT remnant flux or unipolar half-wave current. Thus, a measurement from an IT at a terminal bus of a generator can be adequately represented mathematically using (3).

$$s(t) = \sum_{i=1}^{n} s_i \sin(\omega_i t + \phi_i) + s_{\mathrm{DC}} e^{-t/\tau_{\mathrm{DC}}} + \eta_e \tag{3}$$

where, s_i, ω_i and ϕ_i are the amplitude, frequency and phase of the i^{th} harmonic component in the signal $s(t)$. s_{DC} and τ_{DC} are the DC term parameters in the signal $s(t)$ whereas η_e represents the noise and associated distortions in the signal $s(t)$.

IV. Robust **A**daptive **D**etection **S**cheme (**ADS**)

The schematic of the proposed ADS is shown in Fig. 1. The analogue voltage and current measurements obtained from the ITs serve as inputs for the ADS (detailed below) to output the signal parameter (amplitude, frequency and phase)

estimates. The signal parameter estimation laws are derived by expanding equation (3) as follows to (4).

$$s(t) = \sum_{i=1}^{n} s_{ci}\sin(\omega_i t) + s_{si}\cos(\omega_i t) + s_{\mathrm{DC}}e^{-\tau_{\mathrm{DC}}^{-1}t} + \eta_e$$
$$s(t) = \Theta^{\mathrm{T}}\mathbb{S} + \eta_e \quad (4)$$

$\mathbb{S} = [\sin(\omega_1 t), \cos(\omega_1 t) \dots \sin(\omega_n t), \cos(\omega_n t), 1, (-t)]^{\mathrm{T}}$, and $\Theta = [s_{c1}\ s_{s1}\ s_{c2}\ s_{s2} \dots s_{cn}\ s_{sn}\ s_{\mathrm{DC}}\ s_{\mathrm{DC1}}]^{\mathrm{T}}, s_{ci} = s_i\cos\phi_i$, $s_{si} = s_i\sin\phi_i$, $s_{\mathrm{DC1}} = s_{\mathrm{DC}}\tau_{\mathrm{DC}}^{-1}$, $i = 1, \dots, n$, $\omega_i = i\omega_1$. Θ is a vector of unknown parameters, which needs to be estimated online, with its estimate is denoted as follows.

$$\hat{s} = \widehat{\Theta}^{\mathrm{T}}\mathbb{S};\ \widehat{\Theta}^{\mathrm{T}} = [\hat{s}_{c1}\ \hat{s}_{s1}\ \hat{s}_{c2}\ \hat{s}_{s2} \dots \hat{s}_{cn}\ \hat{s}_{sn}\ \hat{s}_{DC}\ \hat{s}_{DC1}]. \quad (5)$$

The CT/PT measurement signal $s(t)$ is observed through an unknown transfer function $\mathrm{G}(s)$, which represents the linear dynamics of the instrumentation chain. ADS observer removes the requirement of MCTFI [13] in the update laws. Therefore,

$$z - \hat{z} = \mathrm{G}(s)\cdot\tilde{\mathrm{A}} \quad (6)$$
$$\tilde{\mathrm{Z}} = \mathrm{G}(s)\cdot\tilde{\mathrm{A}} = -\mathrm{G}(s)\cdot\tilde{\Theta}^{\mathrm{T}}\tilde{\mathbb{S}} - \mathrm{G}(s)\cdot\tilde{\eta}_e \quad (7)$$

where, $\tilde{\mathrm{Z}} = \mathcal{L}(\tilde{\mathrm{z}}), \tilde{\mathrm{z}} = \mathrm{z} - \hat{\mathrm{z}}$, $\tilde{\mathrm{A}} = \mathcal{L}(\tilde{s}), \tilde{s} = s(t) - \hat{s}$, $\tilde{\Theta} = \widehat{\Theta} - \Theta$, $\tilde{\mathbb{S}} = \mathcal{L}(\mathbb{S})$ and $\tilde{\eta}_e = \mathcal{L}(\eta_e)$. $\mathcal{L}$ denotes the Laplace transform. The unknown transfer function $\mathrm{G}(s)$ is a 'proper transfer function' (PTF) [19]. State space representation of the proper transfer function ($\mathrm{G}(s) = \mathrm{C}(s\mathrm{I} - \mathrm{A})^{-1}\mathrm{B}$) is given below by (8):

$$\dot{\gamma} = \mathrm{A}\gamma + \mathrm{B}\beta, \quad \tilde{\mathrm{z}} = \mathrm{C}\gamma \quad (8)$$

where, $\beta = -\mathbb{S}^{\mathrm{T}}\tilde{\Theta} + \eta_e$, γ is an intermediate variable vector. A Lyapunov function candidate $\mathcal{T}(\tilde{\Theta}, \gamma)$ considered to derive the parameter estimation law is given by (9).

$$\mathcal{T}(\tilde{\Theta}, \gamma) = 0.5(\gamma^T\mathcal{M}\gamma) + 0.5(\tilde{\Theta}^{\mathrm{T}}\Lambda^{-1}\tilde{\Theta}) \quad (9)$$

where, $\mathcal{M}$ is real and strictly positive matrix (RSP) and accounts for the positive definiteness of the function $\mathcal{T}(\tilde{\Theta}, \gamma)$ and Λ is an adaptive-gain matrix.

Lemma 1 [19]: If the sensor transfer function $\mathrm{G}(s)$ is RSP, then there exists a positive scalar ρ, a matrix $\mathcal{M}^T = \mathcal{M} > 0$ and a vector $\boldsymbol{q}$ which satisfies the following equations.

$$\mathrm{A}^{\mathrm{T}}\mathcal{M} + \mathcal{M}\mathrm{A} = -\boldsymbol{q}^{\mathbf{T}}\boldsymbol{q} - \rho\mathcal{N}\ ;\ \mathcal{M}\mathrm{B} - \mathrm{C}^{\mathrm{T}}{=}0 \quad (10)$$

where, matrix $\mathcal{N} = \mathcal{N}^{\mathrm{T}} > 0$.

Using Lemma 1, the dependence of update laws for estimation of parameters upon intermediate vector γ can be disregarded/waived off. As $\tilde{\mathrm{z}}\eta_e$ is very small, therefore,

$$\dot{\mathcal{T}}(\tilde{\Theta}, \gamma) = -0.5\gamma^{\mathrm{T}}\boldsymbol{q}^{\mathbf{T}}\boldsymbol{q}\gamma - 0.5\rho\gamma^{\mathrm{T}}\mathcal{N}\gamma - \tilde{\mathrm{z}}\tilde{\Theta}^{\mathrm{T}}\mathbb{S} + \tilde{\Theta}^{\mathrm{T}}\Lambda^{-1}\dot{\tilde{\Theta}} \quad (11)$$

Parameter estimation law (12) ensures the negative semi-definiteness (NSD) of the $\dot{\mathcal{T}}(\tilde{\Theta}, \gamma)$ (13).

$$\dot{\tilde{\Theta}} = \Lambda\tilde{\mathrm{z}}\mathbb{S} \Rightarrow \dot{\hat{\Theta}} = \Lambda\tilde{\mathrm{z}}\mathbb{S} \quad (12)$$
$$\dot{\mathcal{T}}(\tilde{\Theta}, \gamma) = -0.5(\gamma^{\mathrm{T}}\boldsymbol{q}^{\mathbf{T}}\boldsymbol{q}\gamma) - 0.5\rho(\gamma^{\mathrm{T}}\mathcal{N}\gamma) \quad (13)$$

where, $\Lambda = \mathrm{diag}(\lambda_{c1}\ \lambda_{s1}\ \lambda_{c2}\ \lambda_{s2} \dots \lambda_{cn}\ \lambda_{sn}\ \lambda_{\mathrm{DC}})$ and $\Lambda > 0$. It is deduced from (9)-(13) that $\tilde{\mathrm{z}}, \gamma, \tilde{\Theta}, \widehat{\Theta}, \mathcal{T} \in \mathbf{L}_\infty$ [19].

$$\therefore \lim_{t\to\infty} \mathcal{T}(\tilde{\Theta}(t), \gamma(t)) = \mathbf{L}_\infty < \infty \quad (14)$$

Therefore, the individual update laws for estimation of signal parameters as deduced from (12) are given by (15).

$$\dot{\hat{s}}_{c1} = \lambda_{c1}\tilde{\mathrm{z}}\sin(\omega_1 t), \dot{\hat{s}}_{s1} = \lambda_{s1}\tilde{\mathrm{z}}\cos(\omega_1 t), \dots$$
$$\dot{\hat{s}}_{cn} = \lambda_{cn}\tilde{\mathrm{z}}\sin(\omega_n t), \dot{\hat{s}}_{sn} = \lambda_{sn}\tilde{\mathrm{z}}\cos(\omega_n t), \dots$$
$$\dot{\hat{s}}_{\mathrm{DC}} = \lambda_{\mathrm{DC}}\tilde{\mathrm{z}}\ , \dot{\hat{s}}_{\mathrm{DC1}} = -\lambda_{\mathrm{DC1}}\tilde{\mathrm{z}}t \quad (15)$$

The vector "$\mathbb{S}$" should also satisfy the condition for *excitation persistence* to ensure rapid convergence of signal parameter estimates [19]. A function $\mathbb{S}: \Re^+ \to \Re^n$ is excited persistently in $\Re^n$ if there exist constants "ζ_0", "ζ_1", and "τ_0" such that

$$\zeta_0 I \le \mathrm{I}_{\mathrm{PE}} = \tau_0^{-1}\int_t^{t+\tau_0} \mathbb{S}(\tau)\mathbb{S}^{\mathrm{T}}(\tau)\,\mathrm{d}\tau \le \zeta_1 I \quad (16)$$

Ignoring the presence of permanent DC component in the CT/PT measurements, the PE condition (16)-(17) can be proven. For signals acquired from CTs/PTs, it is a realistic assumption as the DC component ($s_{\mathrm{DC}}(t) = s_{\mathrm{DC}}e^{-t/\tau_{\mathrm{DC}}}\ \forall\ t$) is a decaying exponential function. In this context, the matrix "$\mathbb{S}\mathbb{S}^{\mathrm{T}}$" is a square matrix whose elements are combination of following sinusoidal functions:

$$\cos(\omega_i t), \sin(\omega_i t), \sin^2(\omega_i t), \cos^2(\omega_i t), \cdots$$
$$\cos(\omega_i t)\sin(\omega_i t), \cos(\omega_i t)\sin(\omega_j t), \sin(\omega_i t)\sin(\omega_j t) \cdots$$
$$\cos(\omega_i t)\cos(\omega_j t),\ i, j \in [1\ n] \text{ and } i \ne j$$

with $\tau_0 = 2\pi/\omega_1$, On solving (16) we get,

$$\mathrm{I}_{\mathrm{PE}} = \begin{bmatrix} \pi/\omega_1 & 0 & \cdots & 0 \\ 0 & \pi/\omega_1 & \cdots & 0 \\ \vdots & \vdots & \ddots & \vdots \\ 0 & 0 & \cdots & \pi/\omega_1 \end{bmatrix} \quad (17)$$

Therefore, the proposed design scheme satisfies the PE property (16) with $\zeta_1 \ge \pi/\omega_1$ and $0 < \zeta_0 \le \pi/\omega_1$. Moreover, the "$\mathbb{S}$" and its derivative are bounded vectors with sinusoidal elements i.e., $\dot{\mathbb{S}}, \mathbb{S}, \in \mathbf{L}_\infty$. Satisfying these conditions (PE property and $\dot{\mathbb{S}}, \mathbb{S}, \in \mathbf{L}_\infty$), the convergence of the parameter estimates is guaranteed at an exponential speed. Therefore,

$$\hat{s}_{c1} = \lambda_{c1}\mathrm{S}_\int = \lambda_{c1}\int_t\{\tilde{\mathrm{z}}\sin(\omega_1 t)\}dt \quad (18)$$
$$\hat{s}_{s1} = \lambda_{s1}\mathrm{C}_\int = \lambda_{s1}\int_t\{\tilde{\mathrm{z}}\cos(\omega_1 t)\}dt \quad (19)$$
$$\hat{s}_1^2 = \{\lambda_{c1}\mathrm{S}_\int\}^2 + \{\lambda_{s1}\mathrm{C}_\int\}^2 \quad (20)$$
$$\hat{\phi}_1 = sin^{-1}(\hat{s}_{s1}/s_1) \quad (21)$$

Phasor frequency ($f = \omega_1/2\pi$) estimation law (24) is derived by minimizing the quadratic cost function (22).

$$\mathcal{J} = 0.5\mathcal{E}^2 = 0.5(\hat{s} - s)^2 \text{ where, } \mathcal{E} = (\hat{s} - s) \quad (22)$$
$$\therefore \dot{\hat{\omega}}_1 = -\eta_\omega\partial\mathcal{J}/\partial\omega_1 \quad (23)$$
$$\Rightarrow \dot{\hat{\omega}}_1 = -\eta'_\omega\mathcal{E}\sum_{k=1}^{n}\{\hat{s}_{ck}kt\cos(k\omega_1 t) - \hat{s}_{sk}kt\sin(k\omega_1 t)\}$$
$$\approx -\eta^*_\omega\tilde{\mathrm{z}}\sum_{k=1}^{n}\{\hat{s}_{ck}kt\cos(k\omega_1 t) - \hat{s}_{sk}kt\sin(k\omega_1 t)\} \quad (24)$$

where, η^*_ω is obtained from the stability/convergence analysis theorem (Theorem 1). The negative semi-definiteness (NSD) of the Lyapunov function (9)-(13)and PE condition (16) for parameter convergence have been proven theoretically using (17), as explained above. Therefore, the estimated signal parameters would ultimately converge to their real values for any value of estimator gain Λ and it is tuned to ensure fast dynamic response of the parameter estimator. The estimated amplitude and phase are given by (20) and (21). Likewise, the value of η_ω has to be appropriate. A smaller value of η_ω can guarantee convergence but at a very sluggish speed and dynamic estimate of the state vector may not be acceptable [35]. Excessively high η_ω can lead to possible algorithm divergence. Particle swarm optimization was used to obtain the optimal gain value "Λ" with *integral-time-square-error* as cost function to ensure fast parameter convergence [38].

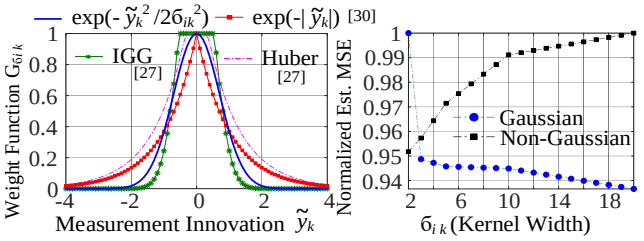

Fig. 2. (*a*) Weight distribution (*b*) Normalized MSE v/s Kernel width.

TABLE I : RSCKF ALGORITHM

Initialization: $\mathcal{P}_\xi^{k-1} = \mathcal{P}_\xi^0, \hat{\boldsymbol{\xi}}_{k-1} = \hat{\boldsymbol{\xi}}_0$

Time Update (Prediction Step)

$\mathcal{P}_\xi^{k-1} = (\mathcal{S}_\xi^{k-1})(\mathcal{S}_\xi^{k-1})^{\mathrm{T}}$

$\mathcal{X}_c^{k-1} = \hat{\boldsymbol{\xi}}_{k-1} + \mathcal{S}_\xi^{k-1}\lambda_\xi;\ c = 1, \cdots, m;\ m = 2n_x$

$\mathcal{X}_c^{k-} = \boldsymbol{f}_p(\mathcal{X}_i^{k-1}, \boldsymbol{u}_{k-1})$

$\lambda_\xi = \begin{cases} \sqrt{n_x}\ ; & c = 1, \cdots, n_x \\ -\sqrt{n_x}\ ; & c = n_x, \cdots, m \end{cases}$

$\hat{\boldsymbol{\xi}}_k^- = m^{-1}\sum_{l=1}^m \mathcal{X}_c^{k-}$

$\mathcal{S}_\xi^{k-} = \boldsymbol{Tria}\left(\left[\mathcal{X}_c^{k+} \quad \mathcal{S}_Q^{k-1}\right]\right)$

$\mathcal{P}_\xi^{k-} = (\mathcal{S}_\xi^{k-})(\mathcal{S}_\xi^{k-})^{\mathrm{T}}, \mathrm{Q}_\xi^{k-1} = (\mathcal{S}_{\mathrm{Q}}^{k-1})(\mathcal{S}_{\mathrm{Q}}^{k-1})^{\mathrm{T}}$

$\mathcal{X}_c^{k+} = m^{-0.5} \times \left[\mathcal{X}_1^{k-} - \hat{\boldsymbol{\xi}}_k^-, \mathcal{X}_2^{k-} - \hat{\boldsymbol{\xi}}_k^-, \ldots, \mathcal{X}_m^{k-} - \hat{\boldsymbol{\xi}}_k^-\right]$

Measurement Update (Correction Step)

$\mathcal{X}_c^k = \hat{\boldsymbol{\xi}}_k^- + \mathcal{S}_\xi^{k-}\lambda_\xi$

$\mathcal{Y}_c^k = \boldsymbol{h}_p(\mathcal{X}_c^k, \boldsymbol{u}_k)$

$\hat{\boldsymbol{y}}_k = m^{-1}\sum_{l=1}^m \mathcal{Y}_c^k$

$\mathcal{S}_{\boldsymbol{y}}^k = \mathbf{Tria}([\mathcal{Y}_c^{k+} \quad \mathcal{S}_{\mathrm{R}}^k]), \mathcal{P}_{\boldsymbol{y}}^k = (\mathcal{S}_{\boldsymbol{y}}^k)(\mathcal{S}_{\boldsymbol{y}}^k)^{\mathrm{T}}$

$\hat{\mathrm{R}}_u^k = (\hat{\mathcal{S}}_{\mathrm{R}}^k)(\hat{\mathcal{S}}_{\mathrm{R}}^k)^{\mathrm{T}} = [\mathcal{S}_R^k]\mathcal{M}_k^{-1}[\mathcal{S}_R^k]^{\mathrm{T}}, \quad \mathcal{M}_k = diag(C_{\sigma 1,k}, C_{\sigma 2,k})$

where, $C_{\sigma 1,k} = e^{-(\mathcal{S}_{\mathrm{R}11}^k \tilde{\mathrm{I}}_{e,k}^2)/(2\sigma_{\mathrm{I}e k}^2)}$, $C_{\sigma 2,k} = e^{-(\mathcal{S}_{\mathrm{R}22}^k \tilde{\mathrm{I}}_{e,k}^2)/(2\sigma_{\mathrm{I}e k}^2)}$, $\mathrm{R}_u^k = (\mathcal{S}_{\mathrm{R}}^k)(\mathcal{S}_{\mathrm{R}}^k)^{\mathrm{T}}$, $\mathcal{S}_{\mathrm{R}11}^k, \mathcal{S}_{\mathrm{R}22}^k$ are diagonal elements in $\mathcal{S}_{\mathrm{R}}^k$.

$$\sigma_{\mathrm{P}e k} = \begin{cases} \sigma_{\mathrm{P}e 0} & if\ \tilde{\sigma}_{\mathrm{P}e k} \geq \sigma_{\mathrm{P}e 0}/\kappa_\sigma \\ \kappa_\sigma \tilde{\sigma}_{\mathrm{P}e k} & if\ \tilde{\sigma}_{\mathrm{P}e k} < \sigma_{\mathrm{P}e 0}/\kappa_\sigma \end{cases}$$

where, $\tilde{\sigma}_{\mathrm{P}e k} = \varrho_e \tilde{\sigma}_{\mathrm{P}e\,k-1} + (1-\varrho_e)|\tilde{\mathrm{P}}_{e\,k}|$

and $$\sigma_{\mathrm{I}e k} = \begin{cases} \sigma_{\mathrm{I}e 0} & if\ \tilde{\sigma}_{\mathrm{I}e k} \geq \sigma_{\mathrm{I}e 0}/\kappa_\sigma \\ \kappa_\sigma \tilde{\sigma}_{\mathrm{I}e k} & if\ \tilde{\sigma}_{\mathrm{I}e k} < \sigma_{\mathrm{I}e 0}/\kappa_\sigma \end{cases}$$

where, $\tilde{\sigma}_{\mathrm{I}e k} = \varrho_e \tilde{\sigma}_{\mathrm{I}e\,k-1} + (1-\varrho_e)|\tilde{\mathrm{I}}_{e\,k}|$

$\mathcal{Y}_c^{k+} = m^{-0.5} \times [\mathcal{Y}_1^k - \hat{\boldsymbol{y}}_k, \mathcal{Y}_2^k - \hat{\boldsymbol{y}}_k, \ldots, \mathcal{Y}_m^k - \hat{\boldsymbol{y}}_k]$

$\mathcal{X}_{c,k}^{++} = m^{-0.5} \times \left[\mathcal{X}_1^k - \hat{\boldsymbol{\xi}}_k^-, \mathcal{X}_2^k - \hat{\boldsymbol{\xi}}_k^-, \ldots, \mathcal{X}_m^k - \hat{\boldsymbol{\xi}}_k^-\right]$

$\mathcal{P}_{\xi y}^k = (\mathcal{X}_{c,k}^{++})(\mathcal{Y}_c^{k+})^{\mathrm{T}},\ \mathcal{Z}_k = \mathcal{P}_{\xi y}^k(\mathcal{P}_{\boldsymbol{y}}^k)^{-1}$

$\mathcal{S}_\xi^k = \mathbf{Tria}\left(\left[\mathcal{X}_{c,k}^{++} - \mathcal{Z}_k\mathcal{Y}_c^{k+} \quad \mathcal{Z}_k\mathcal{S}_{\mathrm{R}}^k\right]\right), \quad \hat{\boldsymbol{\xi}}_k = \hat{\boldsymbol{\xi}}_k^- + \mathcal{Z}_k(\boldsymbol{y}_k - \hat{\boldsymbol{y}}_k)$

A. *Discrete Time Realization/Implementation of* ADS *Scheme*:

To realize the ADS (18)-(24) using a microcontroller or a digital signal processor the parameter estimate is calculated iteratively using the sampled quantities and previous values as follows.

$$\hat{s}_{ci}^k = \hat{s}_{ci}^{k-1} + \mathrm{T_s}\lambda_{ci}\tilde{z}_k \sin(i\omega_1^k(k-1)\mathrm{T_s}) \quad (25)$$

$$\hat{s}_{si}^k = \hat{s}_{si}^{k-1} + \mathrm{T_s}\lambda_{si}\tilde{z}_k \cos(i\omega_1^k(k-1)\mathrm{T_s}) \quad (26)$$

$$\hat{s}_{\mathrm{DC}}^k = \hat{s}_{\mathrm{DC}}^{k-1} + \mathrm{T_s}\lambda_{\mathrm{DC}}\tilde{z}_k \quad (27)$$

$$\hat{s}_{\mathrm{DC1}}^k = \hat{s}_{\mathrm{DC1}}^{k-1} - (k-1)\mathrm{T_s}^2\lambda_{\mathrm{DC1}}\tilde{z}_k \quad (28)$$

$$\hat{f}_1^{k+1} \approx \hat{f}_1^k - 2\pi\mathrm{T_s}\eta_\omega\tilde{z}_k \times \sum_{i=1}^n\{\hat{s}_{ci}^k ik\mathrm{T_s}\cos(ik\omega_1^k\mathrm{T_s}) - \hat{s}_{si}^k ik\mathrm{T_s}\sin(ik\omega_1^k\mathrm{T_s})\} \quad (29)$$

where, T_s is the sampling time.

$$\therefore \hat{s}_1^k = \left(\left(\hat{s}_{ci}^k\right)^2 + \left(\hat{s}_{ci}^k\right)^2\right)^{1/2} \quad (30)$$

and $$\hat{\phi}_1^k = \sin^{-1}(\hat{s}_{s1}^k/\hat{s}_1^k) \quad (31)$$

These laws (25)-(31) can be directly derived from the discrete versions of (9) and (22), given by expressions (32) and (33) below, respectively.

$$\mathcal{J}_k(\widetilde{\Theta}_k, \gamma_k) = 0.5(\gamma_k^{\mathrm{T}}\mathcal{M}\gamma_k) + 0.5(\widetilde{\Theta}_k^{\mathrm{T}}\Lambda^{-1}\widetilde{\Theta}_k) \quad (32)$$

$$\mathcal{J}_k = 0.5\mathcal{E}_k^2 = 0.5(\hat{s}_k - s_k)^2 \quad (33)$$

Theorem 1: The estimated frequency tracks its real time trajectory and the error decays exponentially if η_ω^k satisfies(34), $0 < \beta_f < 2$ and $\eta_\omega^* = \beta_f \mathrm{T_s}^{-1}/\left(\partial\mathcal{E}_k/\partial\hat{\omega}_1^k\right)_{max}^2$

$$0 < \eta_\omega^k = \eta_\omega^* < 2\mathrm{T_s}^{-1}/\left(\partial\mathcal{E}_k/\partial\hat{\omega}_1^k\right)_{max}^2 \quad (34)$$

Proof: Detailed Proof is not provided due to space constraints. Equations (29)-(31) are used to obtain current and voltage phasor parameters (amplitude, frequency and phase) which are then used to generate inputs $\boldsymbol{u}_k = \left[\mathrm{V}_k\ \mathrm{f}_{\mathrm{V},k}\right]$ and measurements $\boldsymbol{y}_k = \left[\mathrm{P}_{e,k}\ \mathrm{I}_{e,k}\right]$ for the DDSE stage.

V. RSCKF BASED DECENTRALIZED DYNAMIC STATE ESTIMATION FRAMEWORK

Nonlinear robust square-root Bayesian filter employing 3rd degree cubature rule has been used to estimate the unobservable internal states of the machine dynamically. This filter, like conventional Bayesian filters, uses two sequential update steps for state estimation: prediction of state vector from the previous estimate and correction using measurement. However, in the measurement update of the RSCKF, the noise covariance matrix 'R_u^k' is modified ($\hat{\mathrm{R}}_u^k$) to account for higher order (non-Gaussian) statistics and counteract the impulsive noise of the measurement vector. $\hat{\mathrm{R}}_u^k$ is derived using a nonlinear regression paradigm (35) of the measurement vector, and is given by (38).

$$\mathrm{Y}_k = \mathrm{H}_k(\boldsymbol{\xi}_k, \boldsymbol{u}_k) + \varepsilon_k, \mathrm{Y}_k = [\mathcal{S}_R^k]^{-\frac{1}{2}}\boldsymbol{y}_k \quad (35)$$

$$\mathrm{H}_k(\boldsymbol{\xi}_k, \boldsymbol{u}_k) = [\mathcal{S}_R^k]^{-\frac{1}{2}}\boldsymbol{h}_p(\boldsymbol{\xi}_k, \boldsymbol{u}_k),\ \varepsilon_k = [\mathcal{S}_R^k]^{-\frac{1}{2}}\boldsymbol{r}_k$$

where, $\mathrm{R}_u^k = (\mathcal{S}_{\mathrm{R}}^k)(\mathcal{S}_{\mathrm{R}}^k)^{\mathrm{T}}$. Then the cost function $\mathbf{J_C}$ (36) is used to obtain the modulated error covariance $\hat{\mathrm{R}}_u^k$.

$$\mathbf{J_C} = \sum_{i=1}^{n_y}\mathbf{G}_{\sigma i\,k} = \sum_{i=1}^{\boldsymbol{n_y}} e^{-\varepsilon_{i\,k}^2/2\sigma_{i\,k}^2} \quad (36)$$

Adapting the similar procedure as in [29], the re-weight matrix $\mathcal{M}_k$ is used to modify the covariance of $\hat{\mathrm{R}}_u^k$ in (38) to limit the variation in innovation vector, ($\tilde{\boldsymbol{y}}_k = \hat{\boldsymbol{y}}_k - \boldsymbol{y}_k$). The variable $\varepsilon_{i\,k}$ is the i^{th} element in $\tilde{\boldsymbol{y}}_k$ at k^{th} instant of time.

$$\mathcal{M}_k = diag(\mathbf{G}_{\sigma 1\,k} \ldots \mathbf{G}_{\sigma n_y\,k}) \quad (37)$$

where, $\mathbf{G}_{\sigma i\,k} = e^{-\varepsilon_{i\,k}^2/2\sigma_{i\,k}^2}$, and $\sigma_{i\,k}$ is the adaptive bandwidth of the kernel and it is used to adjust the distribution width.

$$\hat{\mathrm{R}}_u^k = [\mathcal{S}_R^k][\mathcal{M}_k]^{-1}[\mathcal{S}_R^k]^{\mathrm{T}} \quad (38)$$

In the methods proposed in [15]-[16],[27]-[28], [30] the weight function is tweaked to avoid numerical instability in the inversion process and/or $\sigma_{i\,k}$ is chosen arbitrarily. However, in the proposed methodology, $\hat{\mathrm{R}}_u^k$ (38) is modulated adaptively by the self-tuning weight function $\mathbf{G}_{\sigma i\,k}$ as discussed below (Fig. 2. (*a*)).

A. *Kernel bandwidth* $\sigma_{i\,k}$ *design and RSCKF performance*

The kernel width $\sigma_{i\,k}$ significantly influences the steady state performance and convergence rate of the RSCKF. If $\sigma_{i\,k}$

is too large, RSCKF reduces to a generic CKF and if $б_{i\,k}$ is too small the filter estimate may diverge. As shown in Fig. 2. (*b*), RSCKF performance measured as normalized mean-squared estimation error (MSE) varies with variation in $б_{i\,k}$ for different noise statistics. In the case of Gaussian noise $б_{i\,k}$ should be high for better performance whereas for non-Gaussian noise it should be low. Therefore, the kernel bandwidth $б_{i\,k}$ is designed adaptively to ensure RSCKF performance is better irrespective of the nature of noise statistics. A heuristic for adaptive evolution of $б_{i\,k}$ which ensures enhanced robustness to noise statistics obtained from (36), (A4)-(A9) is given by (39).

$$б_{i\,k} = \begin{cases} б_{i0} & if\ \tilde{б}_{i\,k} \geq б_{i0}/\kappa_б \\ \kappa_б \tilde{б}_{i\,k} & if\ \tilde{б}_{i\,k} < б_{i0}/\kappa_б \end{cases} \tag{39}$$

with, $\tilde{б}_{i\,k} = \varrho_e \tilde{б}_{i\,k-1} + (1-\varrho_e)|\tilde{\boldsymbol{y}}_k|$, $0 < \varrho_e < 1$ whereas $б_{i0} = \kappa_б = 20$. The RSCKF algorithm equations for k^{th} iteration of the DDSE are given in Table-I.

VI. DSE Filter Stability

The choice of filter ensures balanced performance between computational efficacy and ability to deal with strong power system nonlinearities, as detailed in subsequent section. This section addresses the convergence of the DDSE algorithm without any modelling assumptions (unlike[30], [32]).

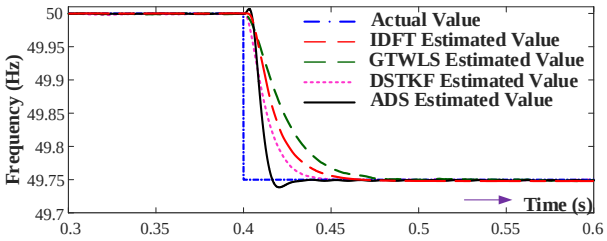

Fig. 3. Convergence/dynamic performance of ADS against other methods.

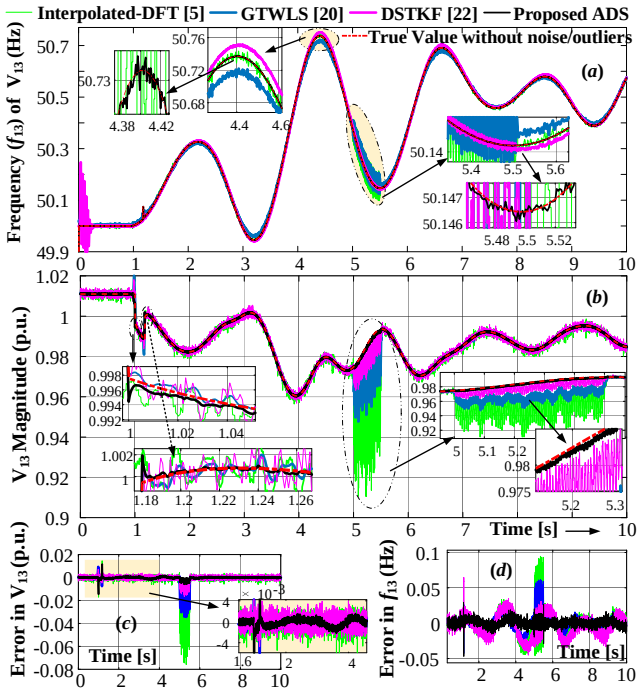

Fig. 4. Estimated parameters and corresponding errors of voltage V_{13}.

TABLE II; Signal Parameter Estimation Errors: 3% Noise

Errors ↓	GTWLS	IDFT-KF	DSTKF	ADS
Max (FE) (Hz)	0.0776	0.0675	0.0651	0.0245
RMSE (FE) (Hz)	0.0295	0.0142	0.0584	0.0039
Max (AE) (p.u.)	0.0126	0.0117	0.0109	0.0062
RMSE (AE) (p.u.)	0.0087	0.0054	0.0025	0.0012

TABLE III : Bias (μ): Standard Error (σ)

$\hat{x}_9$	**HuberM-CKF**		**IDFT-UKF**		**ADS-DDSE**	
	μ	σ	μ	σ	μ	σ
α_9	0.188	0.151	0.188	0.128	**0.033**	**0.057**
ω_9	-0.003	0.001	-0.004	0.001	**0.001**	**0.000**
e'_{d9}	-0.067	0.032	-0.067	0.048	**-0.017**	**0.016**
e'_{q9}	-0.236	0.188	-0.212	0.141	**-0.034**	**0.069**
ψ_{d9}	-0.268	0.218	-0.254	0.164	**-0.028**	**0.054**
ψ_{q9}	0.160	0.090	0.153	0.180	**0.014**	**0.021**
E_{fd9}	-0.122	0.298	-0.098	0.326	**0.002**	**0.024**
$p_{ss1\,9}$	-0.014	0.004	-0.012	0.003	**-0.001**	**0.000**
$p_{ss2\,9}$	-0.024	0.016	-0.026	0.014	**0.005**	**0.004**
$p_{ss3\,9}$	-0.025	0.015	-0.027	0.014	**0.004**	**0.003**

A. *Boundedness of Estimation Error*

Let $\tilde{\boldsymbol{\xi}}_k^- = \boldsymbol{\xi}_k - \hat{\boldsymbol{\xi}}_k^-$, $\tilde{\boldsymbol{y}}_k = \boldsymbol{y}_k - \hat{\boldsymbol{y}}_k$ and $\tilde{\boldsymbol{\xi}}_k = \boldsymbol{\xi}_k - \hat{\boldsymbol{\xi}}_k$ be the prediction, measurement estimation and filtering errors of DDSE respectively. Using Table-I and equations in the Taylor series expansion of (2) around $\hat{\boldsymbol{\xi}}_{k-1}$, we have

$$\tilde{\boldsymbol{\xi}}_k^- = a_k \mathrm{F}_k \tilde{\boldsymbol{\xi}}_{k-1} - a_k \mathrm{F}_k \mathcal{Z}_k \tilde{y}_{k-1} + \boldsymbol{\mathcal{s}}_{k-1} \tag{40}$$

$$\mathcal{P}_\xi^{k-} = [\mathbb{G}]\mathcal{P}_\xi^{k-1}[\mathbb{G}]^T + \mathrm{Q}_k^* \tag{41}$$

where, $\mathbb{G} = a_k \mathrm{F}_k(\mathbf{I} - \mathcal{Z}_k b_k \Omega_k)$, $\tilde{\boldsymbol{y}}_k = b_k \Omega_k \tilde{\boldsymbol{\xi}}_k^- + \boldsymbol{\mathcal{r}}_k$, $\mathrm{F}_k = \left(d\boldsymbol{f}_p(x,u)/dx\right)_{\xi=\hat{\xi}_{k-1}}$, $\Omega_k = \left(d\boldsymbol{h}_p(x,u)/dx\right)_{\xi=\hat{\xi}_k^-}$ where, diagonal matrices a_k, b_k account for system linearization errors and filter tuning. $\mathrm{Q}_k^* = \mathrm{Q}_k + (a_k \mathrm{F}_k \mathcal{Z}_k)\mathrm{R}_k(a_k \mathrm{F}_k \mathcal{Z}_k)^{\mathrm{T}}$. Stability theorem stated below resembles the Theorem 3.1 in [32] (for linear systems) with some simple extensions.

Theorem 2: For a decentralized power system (2), the RSCKF algorithm (Table-I) convergence is guaranteed, i.e., the innovation error ($\tilde{\boldsymbol{y}}_k$) and the estimation error ($\tilde{\boldsymbol{\xi}}_k$) are bounded with certainty $\Rightarrow \lim_{k\to\infty} \tilde{\boldsymbol{y}}_k = \mathbf{0}$ and $\lim_{k\to\infty} \tilde{\boldsymbol{\xi}}_k = \mathbf{0}$.

Proof: The boundedness of $\tilde{\boldsymbol{\xi}}_k^-$, $\tilde{\boldsymbol{y}}_k$ and $\tilde{\boldsymbol{\xi}}_k$ is proven by using equations of the (Table-I), (40)-(41) and considering $\mathcal{L}_k(\tilde{\boldsymbol{\xi}}_k^-) = (\tilde{\boldsymbol{\xi}}_k^-)^T(\mathcal{P}_\xi^{k-})^{-1}(\tilde{\boldsymbol{\xi}}_k^-)$ as a Lyapunov function. Measurement model here is nonlinear. Therefore, the proof here differs from the proofs given in [31], (wherein measurement model is linear and other unrealistic assumptions have been made). It can be proven that the convergence of innovation guarantees the convergence of estimates. A detailed derivation of the proof has been omitted here due to limited space.

VII. Case Studies

The proposed scheme has been tested on a benchmark 16-machine-68-bus test system (Fig. A1 in the Appendix). An ADS based DDSE is located at each machine of the test system, and it estimates the states for the unit dynamically.

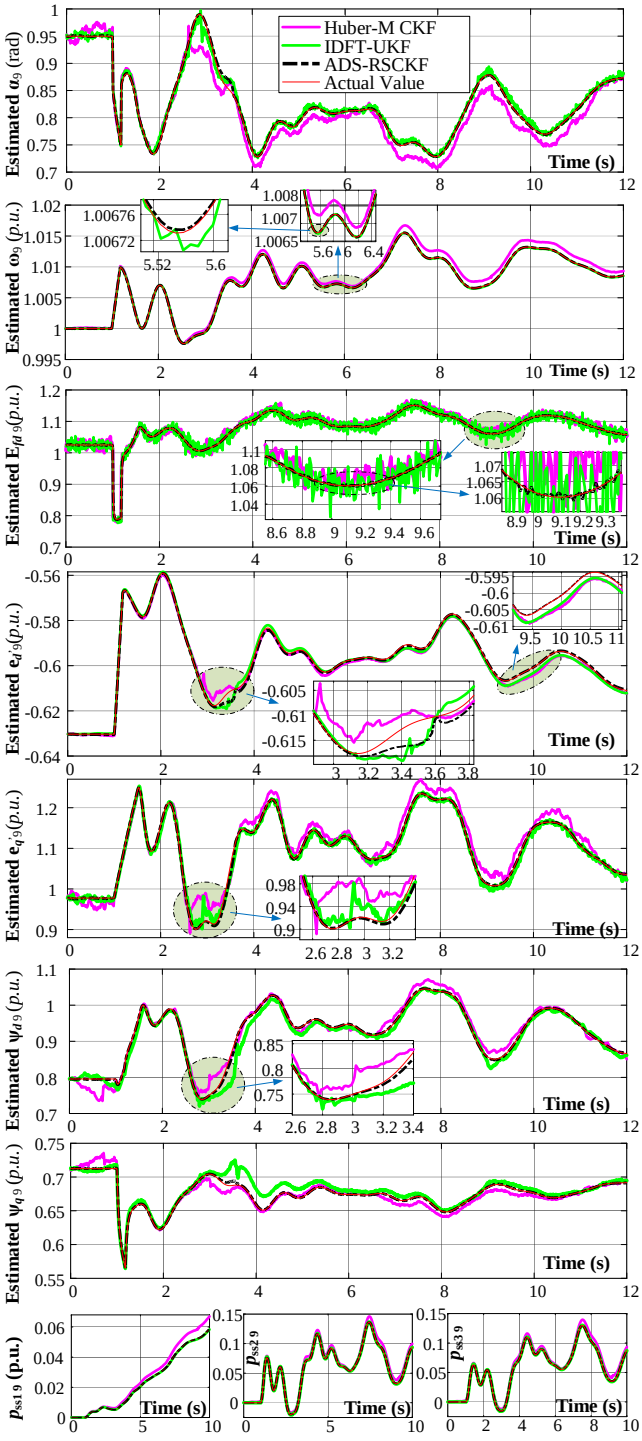

Fig. 5. Comparison of the proposed DDSE scheme with its precursors for 9th unit states for the base case scenario (200 Monte-Carlo runs).

A. *Performance of Adaptive Detection Scheme* (ADS)

The convergence and the dynamic performance of the ADS against its precursors like IDFT [5], GTWLS [20] and DSTKF [22] was evaluated by estimating the frequency of a synthetic signal given by (42) below.

$$s(t) = s_1 sin(2\pi f_1 t + \pi/3) \qquad (42)$$

$$f_1 = \begin{cases} 50Hz & t \leq 4 \\ 49.75\ Hz & t > 4 \end{cases}$$

where, s_1 and f_1 are respectively the amplitude and frequency of this synthetic signal. The frequency estimate trajectory with different methodologies is depicted in Fig. 3. The convergence and the dynamic performance of the proposed ADS is comparatively better.

The preceding stage of the methodology (i.e., ADS) uses instantaneous $V(t)$ and $I(t)$ as measurements, which are produced by adding noise to the analogue values of the current and the voltage of the unit. Dynamic phasor estimation via ADS was further illustrated by estimating the voltage phasor parameters of the 13th generator and subjecting the test system to a bolted 3-phase fault at bus 54 at $t = 1s$ [4]. The fault was cleared at $t = 1.18s$ by opening the faulted tie-line of the double circuit. The estimated parameters are plotted in Fig. 4, wherein the performance of the ADS method is compared to state-of-the-art phasor estimation methodologies, namely, interpolated-DFT [5], generalized Taylor weighted least squares (GTWLS) [20] and DSTKF [22]. A DC bias of magnitude 0.0205 (2%) was added at $t = 5s$ for $0.5s$ to the instantaneous PT measurement to evaluate the robustness of the ADS scheme. The normalized signal parameter errors (both maximum and root-mean-squared values) for 200 Monte-Carlo runs have been tabulated in Table-II. In this table, AE represents the error in the estimated amplitude whereas FE represents the error in the estimated frequency of the signal respectively. The estimation errors with the proposed ADS are marginal compared to its state-of-the-art precursors [5], [20]-[22]. As established through theory and time domain simulations, the ADS is immune to distortions, stepped DC anomalies, and the noise present in the measurements, whereas other direct phasor estimation methods become unstable or do not produce accurate phasor estimates (Fig. 4). Hence, in the subsequent DDSE part, the comparison is made with PMU based DDSEs assuming a maximum total vector error TVE of 1% (although PMUs may also not guarantee 1% TVE under stepped amplitude/phase jumps, DC anomalies and distortions, unlike the proposed ADS method).

B. *Performance of Decentralized Dynamic State Estimator*

The subsequent part uses robust SRCKF whose time step is selected as $0.01s$, as explained in [4]. Therefore, ADS estimates are supplied to the state estimation stage at a sampling time of $0.01s$ via zero order hold (ZOH). For performance comparison, the proposed DDSE scheme is compared with, robust CKF/UKF utilizing Huber function [27]-[28], [31], wherein it uses PMU measurements directly for the estimation of the states, and IDFT-UKF [5], which uses analogue measurements like the proposed DDSE. For base case comparison, the measurement error in the proposed methodology and IDFT-UKF is chosen as 3% as specified by the standards [39]-[40], whereas 1% TVE is chosen for PMU measurements as per IEEE standards [8]. A fast decaying DC component with $s_{DC} = 0.051\ p.u.$ (5%) was also added to the measurements at t=2.5s. The effectiveness of the DDSE methodology was examined by subjecting the steady state system to aforementioned disturbance. Simulated states along with their dynamic estimates, with the proposed scheme and the other schemes for the base case, for the 9th unit have been plotted in Fig. 5. To save space, the plots for other units have not been shown. For 200 Monte-Carlo runs, the bar plots and corresponding probability distribution functions (PDFs) of the errors of the estimated states over the simulated time of 12s for 9th machine are shown in Fig. 6. The Normalized biases μ and

standard errors σ of the estimates for 9th machine are given in Table-III. With the proposed DDSE, the estimated states almost coincide with theoretical values with minimal bias (i.e., the estimates with ADS-DDSE are relatively unbiased) and the standard error (SE) is comparatively low. Therefore, its performance is better in comparison to its precursors for the base case scenario as established by test results.

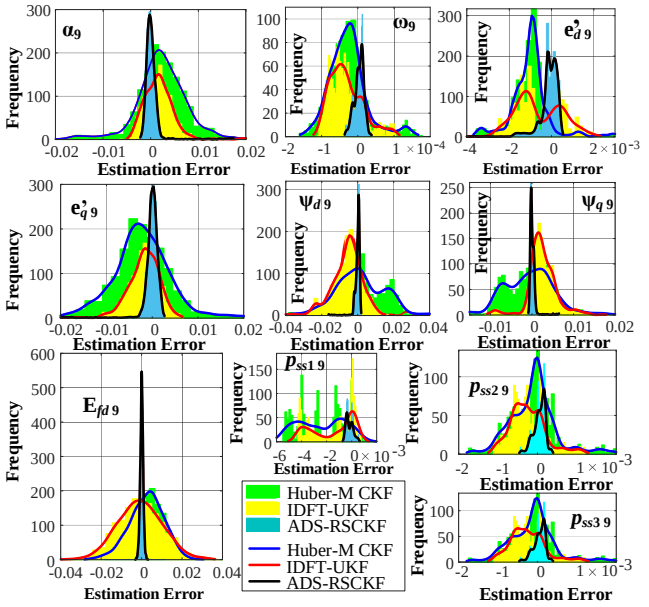

Fig. 6. Bar plots and corresponding PDFs of the estimation errors for 9th unit states for the base case (Gaussian Noise: 200 Monte-Carlo runs).

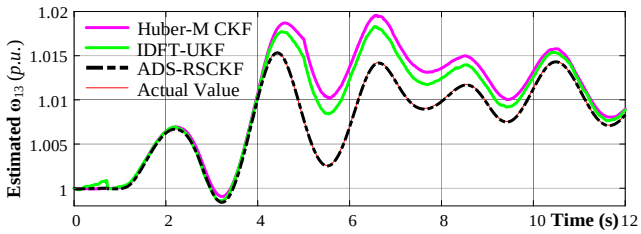

Fig. 7. Estimation of ω_{13} with DC bias in the measurement (V_{13}).

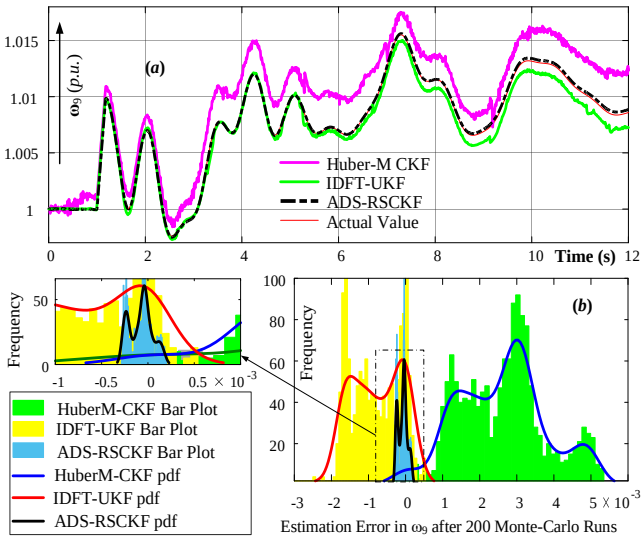

Fig. 8. Comparison of estimation of ω_9 for colored noise for base case

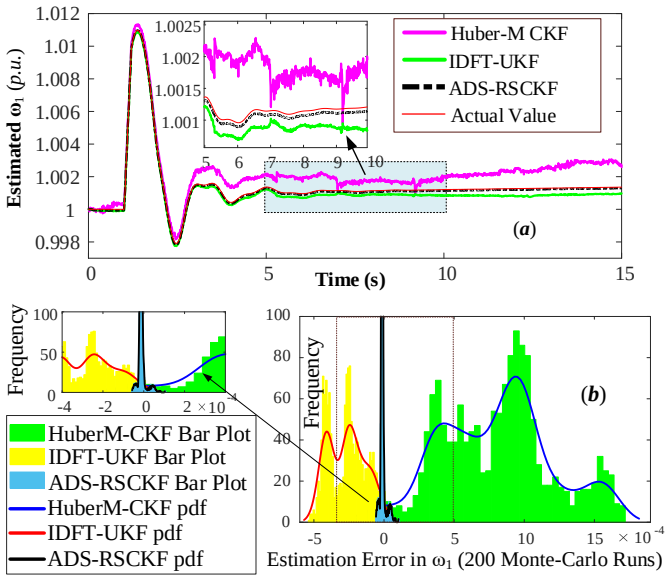

Fig. 9. Two-area system: Comparison of estimation of ω_1 for colored noise.

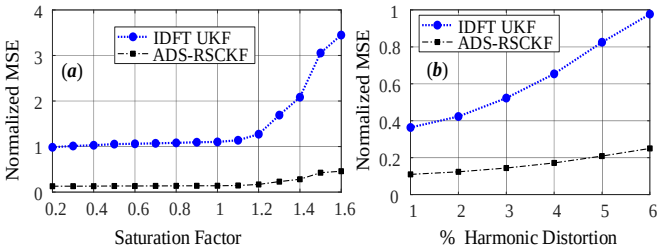

Fig. 10. Effect of instrumentation channel parameter variation (saturation factor) and harmonic distortion on DDSE performance.

C. *Robustness to stepped DC outliers in the Measurement*

The robustness against stepped DC outliers has further been tested by adding -0.011 (10%) DC bias from $t = 4s$ for $1s$ to V_{13} and testing the DDSE performance. The estimates (Fig. 7) with the proposed DDSE are accurate even with stepped outliers in the measurement data.

D. *Robustness to Measurement Noise Characteristics*

Non-Gaussian measurement noise has been used to test the sensitivity of the developed methodology. Estimation plot of ω_9 in the presence of colored noises has been shown in Fig. 8 (a). Corresponding bar plots and PDFs of the estimation error for 200 Monte-Carlo runs is shown in Fig. 8 (b). It is clear from the test results that robust RSCKF based DDSE performs accurately whereas the estimation results in the case of other DDSE algorithms are comparatively inaccurate when the measurement noise is non-Gaussian. It has been further validated by performing a similar test on a 2-area 4-generator benchmark model (Fig. A2 in the Appendix) assuming 3% colored noise contamination of the analogue measurements. In this case, the test system was subjected to a 3-phase fault at bus 9 at t=1s and the fault was cleared at t=1.1s by opening the faulted tie-line of the double circuit. The proposed estimator performance is accurate compared to IDFT-UKF and Huber-M CKF estimators Fig. 9 (*a*)-(*b*).

E. *DDSE Accuracy, Measurement Chain and Harmonics*

Variation in the measurement chain parameters (saturation factor (SF) (Appendix-A), burden resistance, length of the control cables, etc.) impart distortion and have an adverse

impact on the quality of the data [13]-[14]. The saturation factor (SF) of ITs was varied over its range and the DDSE accuracy index (normalized mean square error: NMSE) was plotted (Fig. 10 (*a*)). This index remains constant as long as SF is less than unity and increases marginally as SF is increased beyond unity. The impact of the variation in other parameters of the instrumentation chain is similar. ADS-DDSE is also robust to the harmonic contamination of CT/PT measurements (Fig. 10 (*b*)) and performs better than IDFT-UKF [5].

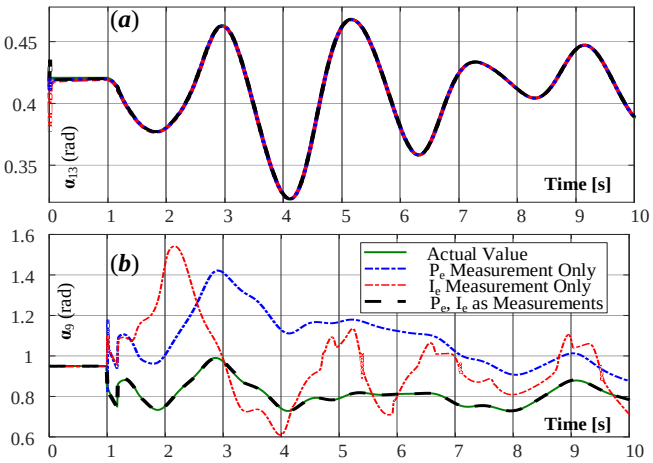

Fig. 11. Observability and Scalability: Estimation of α_{13} and α_9.

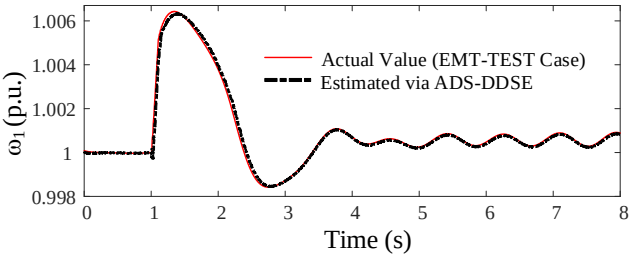

Fig. 12. EMT test case two-area system: Estimation of ω_1 via ADS-DDSE.

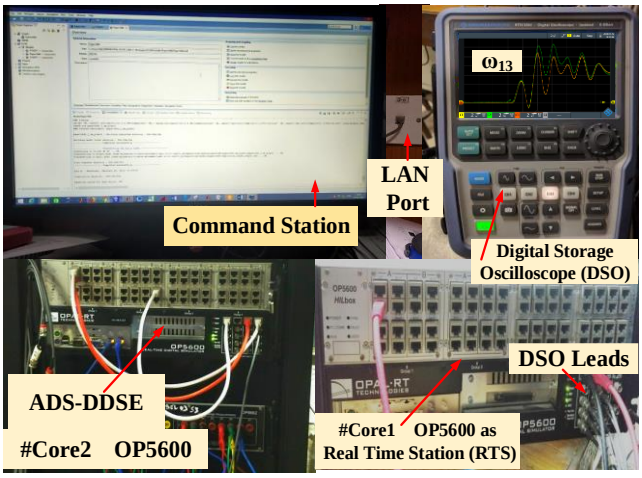

Fig. 13. Scaled Laboratory Setup for real-time implementation using Op5600 multiprocessor.

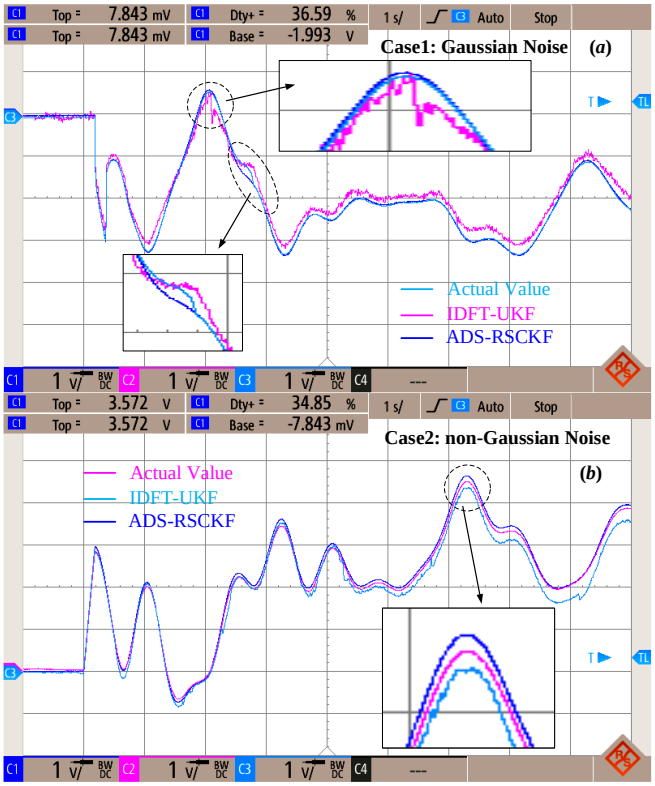

Fig. 14. Real-time results: (*a*): Gaussian Case (*b*) Non-Gaussian Case

F. *Scalability and Observability Condition*

Observability refers to the ability of estimating the state vector in its entirety from the accessible measurement vector whereas scalability refers to robustness of estimation accuracy/quality with an increase in the dimension of the state vector that needs to be estimated. Observability is assessed by checking the rank of the observability matrix "$\mathbb{O}$" [33].

$$\mathbb{O} = \nabla\left\{\left[\mathcal{L}_f^0 \boldsymbol{g} \quad \mathcal{L}_f^1 \boldsymbol{g} \quad \cdots \quad \mathcal{L}_f^{n-1} \boldsymbol{g}\right]^{\mathrm{T}}\right\} \tag{43}$$

where, $\mathcal{L}_f \boldsymbol{g} = \nabla \boldsymbol{g}.\boldsymbol{f}$, $\mathcal{L}_f^0 \boldsymbol{g} = \nabla \boldsymbol{g}$ and $\mathcal{L}_f^i \boldsymbol{g} = \nabla\left(\mathcal{L}_f^{i-1} \boldsymbol{g}\right).\boldsymbol{f}$

If the rank of "$\mathbb{O}$" is n_x, then the system is observable. Based on the rank condition of (43), all the units of the test system are completely observable when P_e and $[P_e \ I_e]^T$ are used as measurement sets separately. However, the numerical observability index [33] is smaller in the case of P_e as measurement and relatively higher when $[P_e \ I_e]^T$ is the measurement vector for 9th unit. For 13th unit with only six states, there is not much difference in the estimation accuracy. Corresponding estimation results (Fig. 11) validate the observability analysis. Despite having full rank of the observability matrix in both the cases, the estimates show weak observability when P_e alone is the measurement for 9th unit. Due to weaker observability, DDSE is very sensitive to measurement noise, and it limits the bad data identification and detection capability and necessitates the use of redundant (or derived) measurements, if available, to improve the estimation accuracy, particularly when the state vector dimension is high.

G. *High Fidelity EMT Models and ADS based DDSE*

The proposed estimator works well even with high fidelity EMTP models. For demonstration, the estimation of a generator-1 (G1) speed of an IEEE 2-Area 4-Generator model using the proposed methodology, and using analogue

measurements acquired from the EMTP model, is shown in Fig. 12. The analogue measurements were contaminated with 3% colored noise as per standards. The accurate estimate of speed illustrates the efficacy and compatibility of the proposed ADS based estimation algorithm with high fidelity EMTP models.

H. *Computational Viability and Real-Time Implementation*

A case study takes 0.79ms per iteration on a workstation computer with i7-10070 CPU, 2.9 GHz processor and 15.8GB usable RAM. Hence, the requirements of computation can be met by an average embedded processor. OP5600 Opal-RT multiprocessors were used to implement the above-mentioned test case scenarios in real-time (RT) Fig. 13. Linux Redhat platform-based Opal-RT processor was used to emulate the system/network dynamics and, therefore, worked as a real-time station and a QNX based OP5600 core was used to realize the ADS-DDSE algorithm. The workstation computer with RT-lab (i7-10070 CPU, 2.9 GHz processor and 15.8GB usable RAM), real-time station (RTS) and QNX core2 (implementing ADS-DDSE method) interact with each other through $100\text{Mbit}/s$ local area network (LAN) based ethernet connection. The OPAL RT-lab central control was utilized to build the "C" code and subsequently used to run this code on multiprocessor of the RTS via a LAN ethernet link. The same central control of the OPAL RT-lab was utilized for code generation for the ADS-DDSE algorithm, and to download it to QNX core2 for executing it in real-time via a LAN ethernet link. The interface between the two multiprocessor cores was setup in analogue domain through built-in DAC/ADC modules, so that it was virtually impossible for the ADS-DDSE estimator to distinguish between the emulated plant and the actual plant. It validates the practical applicability and implementation of the ADS-DDSE in real-time. The test results of the above-mentioned executed scenarios were captured using RT1004 digital storage oscilloscopes as shown in Fig. 14. (a) (wherein 3% Gaussian noise was added to the measurements), Fig. 14. (b) (wherein 3% non-Gaussian noise was added to the measurements). As deduced from the real-time test case scenarios, ADS-DDSE algorithm for estimation of machine states is robust and can be realized using a multiprocessor with similar computational characteristics as Opal-RT processor.

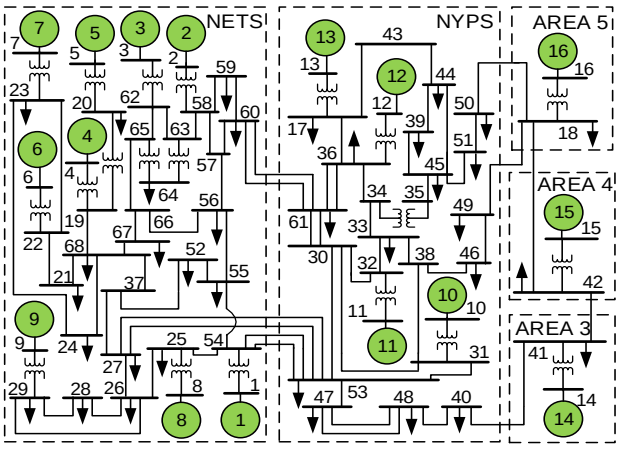

Fig. A1: Simplified line diagram of the 68 bus test system [44]

VIII. Conclusion

ADS based DDSE methodology employing adaptive RSCKF with qualities like numerical accuracy, filter stability, robustness and swift convergence has been presented in this work. It has been implemented at each machine of the interconnected power system and it uses local analogue measurements for estimating the interior states of the synchronous machine dynamically. Proposed ADS-DDSE methodology is immune to synchronization errors, harmonics, noise statistics and DDAs. The proposed DDSE is computationally less intensive and can be realized using an ordinary microcontroller. Benchmark power system was used to test the effectiveness of the scheme. It is well suited for a range of power system control [12], [30], [34]-[35] and protection applications [42]-[43].

Appendix A

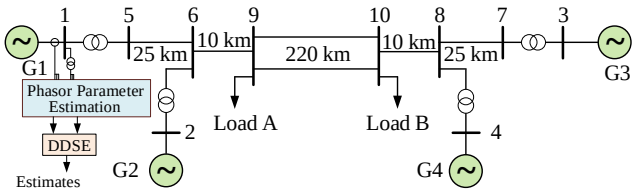

Fig. A2: Simplified line diagram of the two-area test system [44]

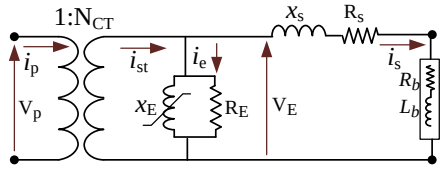

Fig. A3: IEEE PSRC recommended CT model [36], [37]

IEEE PSRC recommended CT model is shown in Fig. A3. The saturation and hysteresis characteristics of the CT is appropriately captured in the transmitted signal on the secondary side $i_s(t)$ (A1) when the excitation current $i_e(t)$ is given by (A2).

$$i_s(t) = i_p(t)/\mathrm{N_{CT}} - i_e(t) \tag{A1}$$

$$i_e(t) = \frac{10(2\pi f)^S |\lambda_e(t)|^S sgn(\lambda_e(t))}{\left(\sqrt{2}\mathrm{V}_E\right)^S R_p} \tag{A2}$$

$$\lambda_e(t) = \lambda_e(t-1) + \Delta\lambda_e(t-1) \tag{A3}$$

where,

$$\Delta\lambda_e(t) = \frac{R_b(i_s(t) - i_e(t)) + L_b di_s/dt}{1 + L_b S|\lambda_e(t)|^{S-1} 10(2\pi f)^S / \left(\left(\sqrt{2}\mathrm{V}_E\right)^S R_p\right)} \Delta t$$

and $R_p = \sqrt{\frac{1}{2\pi}\int_0^{2\pi} sin^{2S}(2\pi f t)dt}$

where, $i_s(t)$ is the current transformer secondary current, $i_e(t)$ is the CT exciting current whereas $i_p(t)$ is the CT primary current. $\mathrm{N_{CT}}$ is the turns ratio of the CT, $\lambda_e\ (t)$ is the flux, R_b and L_b represent the burden resistance and the burden inductance respectively, S is the excitation curve slope, V_E is the exciting voltage at the rated exciting current whereas Δt is the time step of the integration.

Saturation factor (SF): The ratio of voltage of an IT on the secondary side to voltage on the primary side is called saturation factor (SF). When SF is more than unity, it specifies the transformer core is saturated and the secondary side waveshape is significantly distorted.

Derivation of expression for adaptive Gaussian kernel width $б_{i\,k}$.

From equation (36) we have,

$$\mathbf{J_C} = \sum_{i=1}^{n_y} \mathbf{G}_{бi\,k} = \sum_{\boldsymbol{i=1}}^{\boldsymbol{n_y}} e^{-\varepsilon_{i\,k}^2/2б_{i\,k}^2} \tag{A4}$$

For optimal value derivation of individual Gaussian kernel [45], $\partial \mathbf{G}_{бi\,k}/\partial \varepsilon_{i\,k} = 0$. Therefore,

$$\partial \mathbf{G}_{бi\,k}/\partial \varepsilon_{i\,k} = \partial\left(e^{-\varepsilon_{i\,k}^2/2б_{i\,k}^2}\right)/\partial \varepsilon_{i\,k} = 0 \tag{A5}$$

$$= \varepsilon_{i\,k} б_{i\,k}^{-3}(б_{i\,k} - \varepsilon_{i\,k}\partial б_{i\,k}/\partial \varepsilon_{i\,k}) e^{-\varepsilon_{i\,k}^2/2б_{i\,k}^2} = 0$$

Since $б_{i\,k} > 0$, therefore,

$$б_{i\,k} - \varepsilon_{i\,k}\partial б_{i\,k}/\partial \varepsilon_{i\,k} = 0$$

$$\therefore \partial \varepsilon_{i\,k}/\varepsilon_{i\,k} = \partial б_{i\,k}/б_{i\,k}$$

$$\Rightarrow ln(б_{i\,k}) = ln(k_б \varepsilon_{i\,k})$$

$$\Rightarrow б_{i\,k} = k_б|\tilde{\mathbf{y}}_k|, \because\ б_{i\,k} > 0 \tag{A6}$$

where, $k_б$ is a positive constant. To enhance the robustness of a simplistic heuristic (A6) against impulsive outliers, $б_{i\,k}$ is given by

$$\Rightarrow б_{i\,k} = k_б \tilde{б}_{i\,k}, \because\ б_{i\,k} > 0 \tag{A7}$$

where,

$$\tilde{б}_{i\,k} = ϱ_e \tilde{б}_{i\,k-1} + (1 - ϱ_e)|\tilde{\mathbf{y}}_k|,\ 0 < ϱ_e < 1 \tag{A8}$$

Therefore for robustness against both Gaussian as well as non-Gaussian noise $б_{i\,k}$ is given by

$$б_{i\,k} = \begin{cases} б_{i0} & if\ \tilde{б}_{i\,k} \geq б_{i0}/\mathbb{k}_б \\ \mathbb{k}_б \tilde{б}_{i\,k} & if\ \tilde{б}_{i\,k} < б_{i0}/\mathbb{k}_б \end{cases} \tag{A9}$$

REFERENCES

[1] P. Kundur and C. Taylor, "Blackout Experiences and Lessons, Best Practices for System Dynamic Performance, the Role of new Technologies," *IEEE Task Force Report*, 2007.

[2] E. Ghahremani and I. Kamwa, "Online State Estimation of a Synchronous Generator Using Unscented Kalman Filter From Phasor Measurements Units," *IEEE Trans. on Energy Convers*., vol. 26, no. 4, pp. 1099-1108, Dec. 2011

[3] J. B. Zhao *et al*., "Power system dynamic state estimation: Motivations, definitions, methodologies and future work," *IEEE Trans. Power Syst*., vol. 34, no. 4, pp. 3188–3198, Jul. 2019.

[4] A. K. Singh and B. C. Pal, "Decentralized dynamic state estimation in power systems using unscented transformation," *IEEE Trans. Power Syst.*, vol. 29, no. 2, pp. 794–804, Mar. 2014.

[5] A. K. Singh and B. C. Pal, "Decentralized robust dynamic state estimation in power systems using instrument transformers," *IEEE Trans. Signal Process*., vol. 66, no. 6, pp. 1541–1550, Mar. 2018.

[6] A. G. Phadke and J. S. Thorp, *Synchronized Phasor Measurements and Their Applications*. New York, NY, USA: Springer, 2008.

[7] M. S. Almas, L. Vanfretti, R. S. Singh, and G. M. Jonsdottir, "Vulnerability of synchrophasor-based WAMPAC applications' to time synchronization spoofing," *IEEE Trans. on Smart Grid*, 2017.

[8] *IEEE Standard for Synchrophasor Measurements for Power Systems*, IEEE Std. C37.118.1–2011, Dec. 2011.

[9] S. Wang, J. Zhao, Z. Huang, and R. Diao, "Assessing Gaussian assumption of PMU measurement error using field data," *IEEE Trans. Power Del*., vol. 33, no. 6, pp. 3233–3236, Dec. 2017.

[10] S. Särkkä, *Bayesian Filtering and Smoothing*. New York, NY, USA: Cambridge Univ. Press, 2013.

[11] M. T. Menegaz, J. Y. Ishihara, G. A. Borges, and A. N. Vargas, "A systematization of the unscented Kalman filter theory," *IEEE Trans. Autom. Control*, vol. 60, no. 10, pp. 2583–2598, Oct. 2015.

[12] A. K. Singh and B. C. Pal, "Decentralized Control of Oscillatory Dynamics in Power Systems Using an Extended LQR," in *IEEE Trans. on Power Syst.*, vol. 31, no. 3, pp. 1715-1728, May 2016.

[13] T. K. Hamrita, "Repetitive learning control for the correction of wound-type potential transformer measurement errors: sensitivity analysis", *IEEE Trans. on Power Delivery*, vol. 15, pp. 461 – 466.

[14] T. Ahmad and N. Senroy, "Statistical characterization of PMU error for robust WAMS based analytics," *IEEE Trans. Power Syst*., vol. 35, no. 2, pp. 920–928, 2020.

[15] J. Zhao and L. Mili, "Robust unscented Kalman filter for power system dynamic state estimation with unknown noise statistics," *IEEE Trans. Smart Grid*, pp. 1–1, 2017.

[16] J. Zhao, M. Netto and L. Mili, "A Robust Iterated Extended Kalman Filter for Power System Dynamic State Estimation," *IEEE Trans. Power Syst.*, vol. 32, no. 4, pp. 3205-3216, July 2017.

[17] J. Borkowski, D. Kania, and J. Mroczka, "Interpolated-DFT-based fast and accurate frequency estimation for the control of power," *IEEE Trans. Ind. Electron.*, vol. 61, no. 12, Dec. 2014.

[18] G. Yin, L. Guo, and X. Li, "An amplitude adaptive notch filter for grid signal processing," *IEEE Trans. Power Electron*., vol. 28, no. 6, pp. 2638– 2641, Jun. 2013.

[19] A. Loannou and S. Jing, *Robust Adaptive Control*. North Chelmsford, MA, USA: Courier Corporation, 2013.

[20] D. Belega, D. Fontanelli, and D. Petri, "Dynamic phasor and frequency measurements by an improved Taylor weighted least squares algorithm," *IEEE Trans. Instrum. Meas*., vol. 64, no. 8, pp. 2165–2178, Aug. 2015.

[21] S. H. Kang "Fourier transform-based phasor estimation method and apparatus capable of eliminating influence of exponentially decaying dc offsets," U.S. Patent 8, 145, 443, Mar. 27, 2012.

[22] C. Huang, X. Xie and H. Jiang, "Dynamic Phasor Estimation Through DSTKF Under Transient Conditions," *IEEE Trans. Instrum. Meas.*, vol. 66, no. 11, pp. 2929-2936, Nov. 2017.

[23] Y. Y. Hong and D. W. Wei, ''Compensation of distorted secondary current caused by saturation and remanence in a current transformer,'' *IEEE Trans. Power Del*., vol. 25, no. 1, pp. 47–54, Jan. 2010.

[24] A. Hooshyar and M. Sanaye-Pasand, ''Accurate measurement of fault currents contaminated with decaying DC offset and CT saturation,'' *IEEE Trans. Power Del*., vol. 27, no. 2, pp. 773–783, Apr. 2012.

[25] M. S. Ballal, M. G. Wath and H. M. Suryawanshi, "A Novel Approach for the Error Correction of CT in the Presence of Harmonic Distortion," *IEEE Trans. Instrum. Meas.*, vol. 68, no. 10, pp. 4015-4027, Oct. 2019.

[26] I. Arasaratnam, S. Haykin and T. R. Hurd, "Cubature Kalman Filtering for Continuous-Discrete Systems: Theory and Simulations," *IEEE Trans. on Signal Process*., vol. 58, no. 10, Oct. 2010.

[27] L. Chang and K. Li, "Unified form for the robust Gaussian information filtering based on M-estimate," *IEEE Signal Process. Lett*., vol. 24, no. 4, pp. 412–416, Apr. 2017.

[28] R. Izanloo, S. A. Fakoorian, H. S. Yazdi, and D. Simon, "Kalman filtering based on the maximum correntropy criterion in the presence of non-Gaussian noise," *Proc. Annu. Conf. Inf. Sci. Syst*., 2016.

[29] B. Chen, X. Liu, H. Zhao, and J. C. Principe, "Maximum correntropy kalman filter," *Automatica*, vol. 76, pp. 70–77, 2017.

[30] A. S. Mir, S. Bhasin and N. Senroy, "Decentralized Nonlinear Adaptive Optimal Control Scheme for Enhancement of Power System Stability," *IEEE Trans. Power Syst*., vol. 35, no. 2, March 2020.

[31] J. Zhao, "Power System Dynamic State Estimation Considering Measurement Correlations," *IEEE Trans. on Energy Convers*., vol. 32, no. 4, pp. 1630-1632, Dec. 2017.

[32] K. Xiong, H. Y. Zhang, and C. W. Chan, "Performance evaluation of UKF-based nonlinear filtering," *Automatica*, vol. 42, no. 2, pp. 261–270, Feb. 2006.

[33] A. Rouhani and A. Abur, "Observability analysis for dynamic state estimation of synchronous machines," *IEEE Trans. Power Syst*., vol. 32, no. 4, pp. 3168–3175, Jul. 2017.

[34] A. K. Singh and B. C. Pal, "Decentralized nonlinear control for power systems using normal forms and detailed models," *IEEE Trans. Power Syst*., vol. 33, no. 2, pp. 1160–1172, Mar. 2018.

[35] R. Yan, Z. Y. Dong, T. K. Saha, and R. Majumder, "A power system nonlinear adaptive decentralized controller design," *Automatica*, vol. 46, no. 2, pp. 330–336, Feb. 2010.

[36] D. A. Tziouvaras et al., "Mathematical models for current, voltage, and coupling capacitor voltage transformers," *IEEE Trans. Power Delivery*, vol. 15, no. 1, pp. 62-72, Jan. 2000.

[37] T. Bi, H. Liu, X. Zhou and Q. Yang, "Impact of transient response of instrument transformers on phasor measurements," *IEEE PES Gen. Meeting*, 2010, pp. 1-6.

[38] Z. Giang, "A particle swarm optimization approach for optimum design of PID controller in AVR system," *IEEE Trans. Energy Convers*., vol. 19, no. 2, pp. 384-391, Jun 2004

[39] *IEEE Standard Requirements for Instrument Transformers*, IEEE Std. C57.13–2008, Jul. 2008, pp. c1–82.

[40] *IEC Standard for Instrument Transformers*, IEC Std. 60044, 2003.

[41] *IEEE/IEC International Standard - Measuring relays and protection equipment* - Part 118-1: *Synchrophasor for power systems* -

Measurements, IEC/IEEE 60255-118-1:2018 , (Revision of IEEE Std C37.118.1-2011) vol., no., pp.1-78, 19 Dec. 2018.
[42] J. Zhao *et al*., "Roles of Dynamic State Estimation in Power System Modeling, Monitoring and Operation," *IEEE Trans. Power Syst*., vol. 36, no. 3, pp. 2462-2472, May 2021.
[43] Y. Liu *et al*., "Dynamic State Estimation for Power System Control and Protection," *IEEE Trans. Power Syst*.,, vol. 36, no. 6, pp. 5909-5921, Nov. 2021.
[44] C. Canizares et al., "Benchmark models for the analysis and control of small-signal oscillatory dynamics in power systems," *IEEE Trans. Power Syst*., vol. 32, no. 1, pp. 715–722, Jan. 2017.
[45] F. Huang, J. Zhang, and S. Zhang, "NLMS algorithm based on variable parameter cost function robust against impulsive interferences," *IEEE Trans. Circuits Syst. II*, Exp. Briefs**,** vol. 64, no. 5, pp. 600-604, May 2017.

Abdul Saleem Mir (S'19–M'22) received his B. Tech. degree (Hons.) in Electrical Engineering from National Institute of Technology, Srinagar, J&K, and Ph.D. degree in Electrical Engineering from Indian Institute of Technology Delhi, India, in 2014 and 2020 respectively. He is currently an Assistant Professor in the Department of Electrical Engineering, Indian Institute of Technology Roorkee, India. From October 2020 to December 2021, he was a Research Fellow at the University of Southampton with Imperial College London as collaboration Institute. He is a member of IEEE PES Task Force on Dynamic State and Parameter Estimation and IEEE PES Task Force on Standard Test Cases for Power System State Estimation. He was awarded IEEE PES Working Group Member Recognition Award in 2022 for his contributions to IEEE PES TF on Dynamic State and Parameter Estimation. His research interests include dynamic state estimation and control, power system dynamics and modeling/control of renewable energy systems.

Abhinav Kumar Singh (S'12–M'15) received his B. Tech. degree in Electrical Engg. from Indian Institute of Technology Delhi, India, and Ph.D. degree in EE from Imperial College London, U.K. in 2010 and 2015 respectively. He is a Lecturer at the School of Electronics and Computer Science, University of Southampton. Previously, he was a Lecturer at the University of Lincoln from Aug 2017 to Mar 2019, and a Research Associate at Imperial College London from Jan 2015 to July 2017. He won IEEE PES Working Group Recognition Award in 2016 for his contributions to IEEE PES task force on benchmark systems. He was awarded IEEE PES Working Group Recognition Awards in 2016 and 2022 for his contributions to two IEEE PES Task Forces. He is a member of IEEE PES Task Force on Dynamic State and Parameter Estimation and IEEE PES Task Force on Standard Test Cases for Power System State Estimation. He currently serves as an Editor of IEEE Transactions on Power Systems. His research interests include real-time estimation and control of future energy networks.

Nilanjan Senroy (S'01–M'06-SM'18) received the B. Tech. degree from the National Institute of Technology, Jamshedpur, India, and the M.S. and Ph.D. degrees from Arizona State University, Tempe, AZ, USA. He also has postdoctoral experience at the Center for Advanced Power Systems, Florida State University, Tallahassee, FL, USA. He is currently Power Grid Chair Professor in the Department of Electrical Engineering, Indian Institute of Technology Delhi, India. He currently serves as an Editor of IEEE Transactions on Power Systems and IEEE PES Letters. His research interests include power system stability and control, dynamics, modeling and simulation of wind energy conversion systems and signal processing techniques in power systems.